Principal Component Analysis Applied to Surface Electromyography: A Comprehensive Review

Ganesh R. Naik*, *Senior Member, IEEE*, S. Easter Selvan, Massimiliano Gobbo, Amit Acharyya, *Member, IEEE*, and Hung T. Nguyen, *Senior Member, IEEE*

***Abstract*—Surface electromyography (sEMG) records muscle activities from the surface of muscles, which offers a wealth of information concerning muscle activation patterns in both research and clinical settings. A key principle underlying sEMG analyses is the decomposition of the signal into a number of motor unit action potentials (MUAPs) that capture most of the relevant features embedded in a low-dimensional space. Toward this, the principal component analysis (PCA) has extensively been sought after, whereby the original sEMG data is translated into low-dimensional MUAP components with a reduced level of redundancy. The objective of this article is to disseminate the role of PCA in conjunction with quantitative sEMG analyses. Following the preliminaries on the sEMG methodology and a statement of PCA algorithm, an exhaustive collection of PCA applications related to sEMG data is in order. Alongside the technical challenges associated with the PCA-based sEMG processing, the envisaged research trend is also discussed.**

***Index Terms*—Surface electromyography (sEMG), artificial neural network (ANN), principal component analysis (PCA), motor unit action potential (MUAP), flexions, self-organizing feature map (SOFM), support vector regression (SVR), myoelectric signal.**

I. Introduction

SURFACE ELECTROMYOGRAPHY (sEMG) is the electrical recording of muscle activity from the skin surface. It is the result of superposition of a large number of transients having a semi-random temporal and spatial separation [1]–[3]. These transients are the motor unit action potentials (MUAPs) closely related to the strength of a muscle contraction, which carry abundant information on the motor control. For instance, the sEMG amplitude and frequency have been regarded as indicators of the localized muscular fatigue. The amplitude and spectral information of sEMG have also been exploited to estimate the force of muscle contraction and torque, respectively [4]–[6]. Despite the potential applications of sEMG, the presence of artifacts and noise, especially at a low level of muscle activity make the recordings unreliable. The removal of artifacts and noise is admittedly challenging due to the spectral and temporal overlap as well as the need for separating the relevant signals from other bioelectric ones [6], [7].

The intricate human body anatomy accounts for a significant overlap of a number of muscles, which in turn leads to the crosstalk of activities from muscles in proximity to each other. Moreover, the complex nature of MUAPs contributes to the complexity of an sEMG signal. To this end, numerous techniques are currently being employed that aim to eliminate the noise, artifacts, as well as the crosstalk [8], [9]. Amongst them, a few noteworthy ones are the spectral filtering, wavelet transform, and correlation technique [10]–[12]. The spectral overlap between the sEMG signal and artifacts poses challenges to the effectiveness of spectral filtering. On the upside, wavelets combine the temporal and spectral properties, and hence are suitable for signals that may not be separable using the spectral filtering. However, wavelet approaches are limited to continuous signals with spectral overlaps [8], [13]. The time-frequency analysis offers a map of the temporal localization of a signal's spectral characteristics in the time-frequency domain [11], [14]. The drawback with this scheme is the high-dimensional feature vector, which would warrant an increase in the number of learning parameters of a classifier. In most instances, the aforementioned techniques require the dimensionality of sEMG to be reduced for their efficient performance. Therefore, it is imperative to resort to the dimensionality reduction of the feature vector without compromising on the classification accuracy. Apparently, the dimensionality reduction speeds up the classifier and relaxes its memory requirements [15]–[17].

In this regard, most of the signal processing techniques, developed for sEMG waveform decomposition in the temporal domain, fall under the umbrella of matrix factorization, and are extensions of the factor analysis [18]. These strategies include principal component analysis (PCA), independent component analysis (ICA), singular value decomposition (SVD), and non-negative matrix factorization (NMF) [19]–[22]. Though widely adopted for EMG signal processing, each of these methods has inherent advantages and disadvantages. Conversely, there remains no specific factorization method ideally suited for sEMG applications, and consequently, one must cautiously assess the pros and cons of a method on the basis of the sEMG experiment and the type of features, as well as the dataset to analyze. Nevertheless, when it comes to multi-electrode recordings and a large number of sEMG experiments (datasets), the PCA prevails as the favorite choice owing to its conceptual simplicity, practicability, and the ability to be easily computed by readily available statistical programming

This project was supported by the University of Technology Sydney Chancellor's Post-Doctoral Research Fellowship (Grant CPDRF2013-16).

G. R. Naik and H. T. Nguyen are with the Center of Health Technologies, University of Technology Sydney, 2007, Australia (e-mail: Ganesh.Naik@uts.edu.au; Hung.Nguyen@uts.edu.au).

S. E. Selvan is with the Human Performance and Engineering Research Lab, Kessler Foundation, West Orange, NJ, U.S.A. (e-mail: ESelvan@kesslerfoundation.org).

A. Acharyya is with the Department of Electrical Engineering, Indian Institute of Technology (IIT), Hyderabad, India (e-mail: amit_acharyya@iith.ac.in).

M. Gobbo is with the Department of Clinical and Experimental Sciences, University of Brescia, Brescia, Italy (e-mail: massimiliano.gobbo@unibs.it).

packages. Indeed, the PCA has unanimously been accepted as a potential tool to analyze large datasets of EMG signals derived from multi-electrode recordings in research and clinical settings [15], [23], [24].

The PCA is a linear feature projection method intended for reducing the dimensionality of data. It becomes pervasive in the field of human movement analysis to reveal patterns in data of various kinds, e.g., kinematics, kinetics, EEG, and EMG, as well as to compress the dimension of the multivariate dataset recorded. In principle, the PCA computes a smaller set of basis vectors that defines a low-dimensional space, wherein the multivariate data can be represented such that the resulting patterns preserve most of the relevant features. By virtue of dimensionality reduction, the classifier design is simplified, and the pattern recognition technique is relieved of significant computational burden. Furthermore, the PCA is capable of preserving the underlying pattern of a multivariate time series, and the PCA-reduced features can reasonably approximate the distribution of original features. Nevertheless, a drawback could be that the data corresponding to different classes may not exactly be separated into clusters in the reduced feature space. In other words, the PCA learning merely produces a well-described coordinate system for the distribution of all features, without considering the class separation. On the contrary, the features endowed with a high-class separability do improve the recognition accuracy. Hence, there is an increasing trend to employ the PCA in conjunction with other techniques in most of the sEMG signal processing applications [15], [25], [26].

The intent of this article is to provide a comprehensive overview of the PCA applied to sEMG signal processing, first by outlining the main methodological aspects, and then by summarizing the literature concerning the effective application of PCA in sEMG processing both in research and clinical settings. To this end, the paper has been organized as follows. Section II sets a background on the sEMG and PCA by briefly explaining the sEMG acquisition as well as the PCA algorithm, and by highlighting the relevance of PCA in sEMG analyses. In Section III, the state-of-the-art PC selection procedures are concisely presented, and exemplified using sEMG data pertaining to three hand gesture movements. An exhaustive collection of PCA-based sEMG applications including the assessment of muscle strength, prosthetics, facial, and human movement is tabulated in Section IV. The article is concluded in Section V with future research directions.

II. Preliminaries

Of due relevance here is to provide an overview of sEMG and PCA, and to highlight the suitability of PCA for sEMG processing, prior to delving into the PCA-based sEMG applications.

A. Surface Electromyography

The sEMG, being the non-invasive electrical recording of muscle activities, carries vital information concerning the anatomy and physiology of muscles. In addition, the non-invasive recording procedure obviates the need to penetrate the skin, thereby providing a safe and easy means for signal acquisition [27], [28]. Apropos of a better understanding of the mechanism behind the sEMG recording, a brief description of the anatomy, physiology, and the electrical properties of muscles is in order.

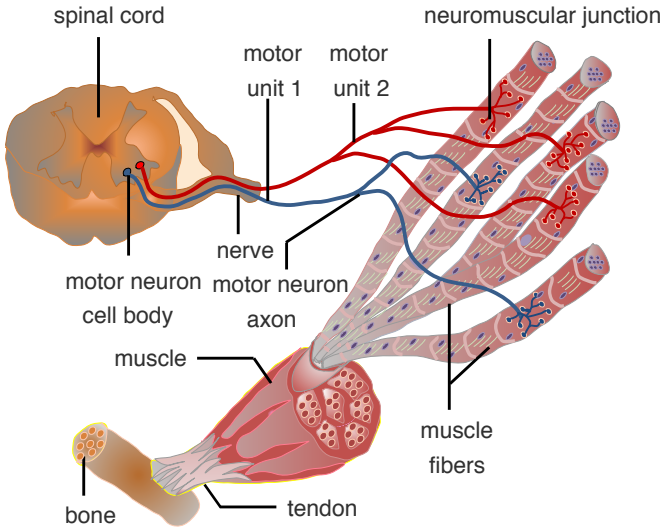

Fig. 1. The motor neuron (red and blue ovoid-shaped minuscule structures embedded in the spinal cord) stimulates muscle fibers (shaded in pink) ranging from 2 to 2000, and they are collectively known as a motor unit. The action potential transmitted by the motor neuron propagates along its axon to the neuromuscular junction, wherein the axon terminal (branches with dots in red and blue) and the motor end plate of the muscle fiber meet to form a synapse [29].

Muscle Structure. A muscle consists of a large number of muscle fibers, which are grouped into several motor units (MUs). An MU is regarded as the basic level of the neuro motor system of a muscle. All the muscle fibers that belong to an MU are controlled by a single motor neuron as shown in Fig. 1. The number of muscle fibers housed in an MU is termed as *innervation ratio*, which in turn differs depending on the type and the function of muscle fibers. For instance, the innervation ratio of muscles that require a fine control, e.g., hand, ocular, and facial muscles, is low (close to 1:5), whereas the muscles requiring only a gross movement, e.g., back or leg antigravity muscles, are endowed with a high innervation ratio (1:2000) [30], [31].

The *neuromuscular junction* (NMJ) is the synapse that develops between a muscle fiber in an MU and the associated motor neuron as illustrated in Fig. 1. The NMJ is located near the middle of a muscle cell, and the region is called the *innervation region*. The muscle fibers that constitute an MU are distributed pseudo-randomly across the cross-section of a muscle to ensure equal distribution of the force generated by each MU [32], [4].

Muscle Contraction. The stimulations from motor neurons cause muscle contractions that fall under three categories: *isometric*, *concentric*, and *accentric*. The muscle contraction that preserves the muscle length is known as the isometric contraction, e.g., contractions related to postural control. The concentric contraction results in the shortening of a muscle; owing to the expenditure of energy toward the reduction

of muscle length, the concentric contraction is vested with less muscular energy than the isometric one. By contrast, the muscle lengthens during the accentric contraction. The concentric and accentric contractions are collectively known as *un-isometric* contractions [33], [34].

Muscle Recruitment Pattern. The manner in which the MUs are selected to participate in a muscle contraction is called the *recruitment process*, and it relies on the "size principle". This means that for a small degree of contraction, the MUs composed of a small number of muscle fibers are engaged; alternatively, larger levels of contraction necessitates the involvement of MUs comprising ample number of muscle fibers. In a contraction that generates a constant force, namely, the *isotonic* contraction, the activation pattern switches from one MU to another so that the MU can evade from growing fatigue [35], [36].

sEMG Signal Generation. A motor neuron stimulates the muscle fibers by sending out the nerve action potential, which travels along the axon towards the muscle fibers. Notwithstanding the fact that the same action potential triggers a set of muscle fibers, their stimulation varies in time, since the axon branch to individual muscle fibers differs in length. This time difference between the activation of muscle fibers is known as *jitter*. The result of depolarization of muscle fibers in an MU due to the stimulus caused by a motor neuron can be considered as a single MUAP. Thus the sEMG signal emerges as the summation of electrical activities from all the active MUs in close proximity to the electrode as illustrated in Fig. 2. The shape and the amplitude of the surface action potential are hence influenced by the properties of body tissues sandwiched between the muscle fibers and the recording electrodes. In particular, the body tissues jointly act as an imperfect insulator with low-pass filter characteristics, and therefore tend to attenuate the high frequency components of the acquired signal [4], [31].

We recall that in sEMG, the non-invasive recording of the muscle activity entails the superposition of a large number of muscle action potentials with a pseudo-random temporal and spatial separation. The origin of each MUAP is inherently random, and the electrical characteristics of the surrounding tissues are non-linear. The ensuing result is that the amplitude of the sEMG signal turns out to be pseudo-random, and its probability distribution function (PDF) resembles a Gaussian function [13], [37], [38].

While one could possibly think of numerous applications involving the sEMG, it must be borne in mind that the sEMG per se may lead to less reliable results. In order to make the best use of the acquired sEMG, the influences due to the following have to be counteracted: anatomy (number, size, and spatial distribution of motor units); physiology (training, disorder, and fatigue); nerve-related aspects (disorder and neuromuscular junction); contraction (level and speed of contraction, isometric/dynamic, and force generated); artifacts (crosstalk between muscle and ECG interference); and recording (procedure, noise, electrode properties—spacing, type, and size of electrodes—as well as recorded sites) [13], [37], [39]. It is viable to alleviate their undesirable impact on the signal to some extent by careful skin preparation and the choice of proper anatomical landmarks for the electrode placement. Note that this adverse effect is more pronounced when the sEMG signal strength remains very small, for instance during a static posture. The sEMG signal can also be categorized with regard to each of these influencing criteria [5], [39], [40].

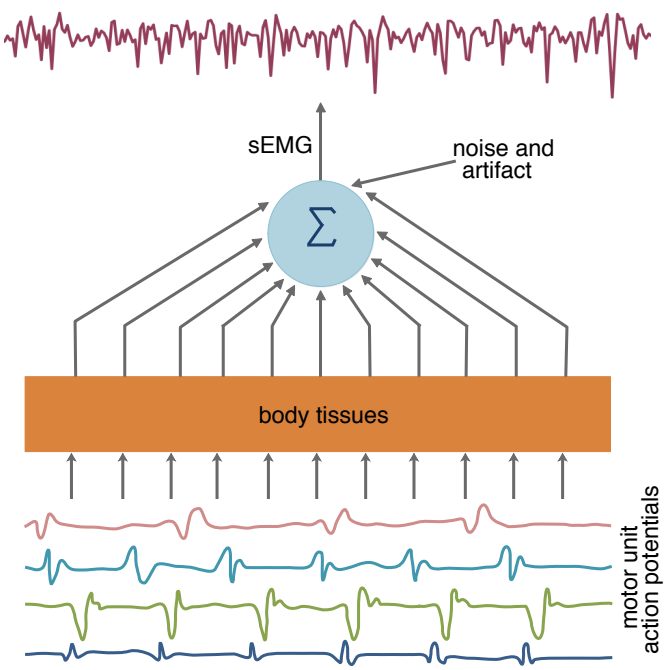

Fig. 2. The sEMG signal is the superposition of all MUAPs in the immediate vicinity of the electrode. Notice that the MUAPs are affected by the electrical characteristics of body tissues interposed between the muscle fibers and the electrode, prior to being summed up.

The sEMG is proven effective in several fields including sports training, rehabilitation, machine and computer control, occupational health and safety, and for identifying posture disorders. Recall from Section I that the sEMG amplitude and frequency have been regarded as indicators of the localized muscular fatigue. As exemplified in [13] and [38], the amplitude and spectral information of sEMG provide cues to estimate the muscle force and muscle voluntary contractions (MVCs). On the other hand, the PCA plays a vital role in retrieving MUAPs from sEMG amidst noise, crosstalk, and artifacts. For completeness sake, a concise description of the PCA technique is provided in the sequel.

B. PCA Fundamentals

The PCA is a simple yet efficient non-parametric approach devoted to render a statistical description of a complex data by revealing the hidden structures and suppressing the noise. This technique, prevalent in many fields, characterizes the data by relying on the second-order statistics, and is acclaimed to yield quite reliable results. More formally, the PCA is an orthogonal linear transformation that decorrelates a multivariate data by projecting it onto a new coordinate system termed as the principal components (PCs). These components can be regarded as a set of spatial directions, onto which the projected data guarantees the maximum variance. Note that there is a natural

way of ordering the PCs based on the variance of the projected data. This means that the variances of the data projected onto the first up to the last component are in the decreasing order. In general, the original data can be well represented with merely a few first PCs [19], [41]–[43].

There are two widely followed approaches to perform the PCA: (i) the *eigenvalue decomposition* of the data covariance matrix; and (ii) the *singular value decomposition* (SVD) of the centered data matrix.

Let the $m \times n$ data matrix be denoted as $\mathbf{X}$ with m and n being the number of samples and the number of variables, respectively. As a preprocessing step, $\mathbf{X}$ is *centered*, meaning that the column-wise mean of $\mathbf{X}$ is subtracted from the elements of the corresponding columns of $\mathbf{X}$. The *covariance matrix* of $\mathbf{X}$ is given by an $n \times n$ symmetrical matrix, defined as $\mathbf{C} = \mathbf{X}^\top\mathbf{X}/(m-1)$, where $(\cdot)^\top$ denotes the transpose of the matrix in the argument. The eigenvalue decomposition diagonalizes $\mathbf{C}$ to yield $\mathbf{V}\mathbf{\Lambda}\mathbf{V}^\top$, where the columns of $\mathbf{V}$ and the diagonal elements λ_i, $i = 1, \ldots, n$, of $\mathbf{\Lambda}$ turn out to be the *eigenvectors* and *eigenvalues* of $\mathbf{C}$, respectively. Note that the eigenvalues of $\mathbf{C}$ are arranged in the decreasing order along the main diagonal of $\mathbf{\Lambda}$, and are associated with the columns of $\mathbf{V}$. This induces a natural ordering of the PCs that are expressed as the columns of $\mathbf{XV}$, whose variances are in the decreasing order as well (refer to the illustration in Fig. 3).

Alternatively, one can perform the singular value decomposition of $\mathbf{X}$ to obtain $\mathbf{USV}^\top$, wherein the diagonal elements s_i, $i = 1, \ldots, n$, of $\mathbf{S}$ are known as the *singular values*. It is straightforward to observe the link between the singular values and the eigenvalues as follows: $\lambda_i = s_i^2/(n-1)$. Furthermore, the PCs can be denoted as the columns of $\mathbf{USV}^\top\mathbf{V} = \mathbf{US}$.

What follows is a brief stepwise procedure on the estimation of PCs for a given multivariate data via eigenvalue decomposition.

- Compute the covariance matrix of the mean-adjusted (centered) data.
- Obtain the eigenvalues and eigenvectors of the data covariance matrix.
- Sort the eigenvalues in the descending order to select the first few "significant" values.
- Form a transformation matrix that comprises the eigenvectors associated with the chosen eigenvalues.
- Project the data onto the transformation matrix.

For a more elaborate treatment on the computation of PCA, one may refer to [19], [43], [44].

C. Relevance of PCA in sEMG Processing

PCA has gained effervescent popularity in dimensionality reduction tasks involving sEMG and prosthetic applications. It plays a crucial role in reducing the dimensionality of a feature space in order to extract the subspace that "best" describes the given data, thereby aiding to recognize patterns. In sEMG-based studies, e.g., studies of human movement, owing to the data redundancy, the PCA has been employed to determine the most important factors that contribute to the sources of variation in movement patterns [23], [45]. As a consequence, the following set of new variables that correlate

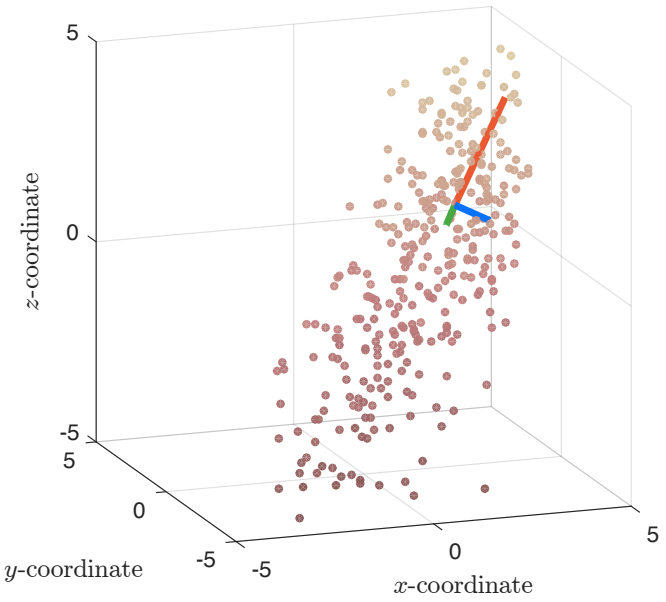

Fig. 3. Each data point shown in pink is a 3-dimensional vector, and 400 such points are displayed in the plot that are randomly drawn from a normal distribution. The 3 PCs are computed for the dataset using the eigenvalue decomposition as discussed in Section II-B, and they are portrayed with line segments in orange, green, and blue color in descending order of their corresponding eigenvalues.

with the original variables is observed: (i) The PCs accounting for a large amount of total variance are presumably related to the control signal outputs of spinal pattern generators, which trigger the corresponding muscles to generate movement under the influence of commands that are sent to the motor units through the descending pathway [46]. (ii) On the other hand, the components that explain only a small amount of the total variance are generally deemed as random noise within the system [41]. The criterion that governs the choice of PCs deduces the number of components in each category. Many studies have successfully demonstrated that the application of PCA to kinematic, kinetic or sEMG data can unveil the underlying coordinative structures in the correlated patterns of variation among joints or body segments [47], [48].

As explained in Section II-B, an EMG dataset $\mathbf{X} \in \mathbb{R}^{p \times q}$ comprising p samples with q variables is first centered, and then its covariance matrix $\mathbf{C} \in \mathbb{R}^{q \times q}$ is computed. Upon the eigenvalue decomposition of $\mathbf{C}$, only $r < q$ columns of $\mathbf{V}$ that correspond to the significant eigenvalues—as determined from the scree-plot of eigenvalues—are selected to extract r number of PCs expressed as the columns of $\mathbf{X}\tilde{\mathbf{V}}$, where the columns associated with insignificant eigenvalues are annihilated from $\mathbf{V}$ to form $\tilde{\mathbf{V}} \in \mathbb{R}^{q \times r}$.

In addition, if $\tilde{\mathbf{V}}$ has robustly been estimated with the help of a large EMG dataset, the dimensionality of a subset of EMG data, $\mathbf{Y} \in \mathbb{R}^{t \times q}$, e.g., the one related to a specific hand gesture or neural disorder, can be reduced by right multiplying $\mathbf{Y}$ by $\tilde{\mathbf{V}}$.

The aforedescribed strategy is a befitting choice in various sEMG applications. For instance, since the dexterity is attributed to only a few control signals in a myoelectric

prosthesis, useful sEMG information such as the degrees of freedom (DoF) of a dexterous robotic hand can be reduced by deploying this *inverse PCA* algorithm. Another noteworthy application would be to reveal the hidden information that underlies a neural disorder data.

III. PC Selection With Illustrations

The ability of PCA to express the sEMG data with a few selected PCs is demonstrated with the following example, wherein the sEMG data pertains to three different hand gestures of varied complexities, i.e., movement involving middle finger alone; index, middle, and ring fingers together (IMR); and hand close (HC) position. For the sake of brevity, we refrain from describing the data collection and preprocessing details, which can be found in [49]. Instead we focus on the optimal choice of the PCs by dint of eigenvalues after decomposing the sEMG data under consideration, each of size $12\,000 \times 8$, with the PCA algorithm. A simple rule-of-thumb has been adhered to in [50] that recommends to retain the PCs with the eigenvalues greater than one; however, as cautioned in [51], this naive strategy may lead to loss of valuable information. Traditionally, one can plot the eigenvalues in decreasing order, and the resulting plot known as the *scree-plot* may be visually inspected to track the *elbow point*, where the slope of the scree-plot undergoes an abrupt transition. Since it is based on visual heuristics, obviously this procedure is highly subjective. In the pursuit of detecting the elbow point by an automatic procedure, statistical approaches have recently been advocated, e.g., the profile likelihood approach in [52]. Nevertheless, given a small sample size, an approach designed to estimate the elbow by maximizing a profile likelihood function may lead to inaccurate results. Another popular method is to retain the smallest number of components that capture an appreciable percentage γ of the total variance; in practice, γ is determined to be 80% or 90%. Note, however, that the choice of γ is not rigorous and is contingent on the application at hand. Alternatively, one can resort to sequential tests, wherein a series of hypothesis tests are sequentially conducted to verify whether the small eigenvalues are equal. The validity of the sequential tests is hinged on the assumption that the underlying data follows a multivariate normal distribution. Furthermore, it is also difficult to approximately predict the overall significance level due to the random number of tests and the fact that the tests do not guarantee to remain independent from each other [43]. Aside from these, the resampling method estimates the null distribution of each PC by resampling the data repeatedly via permutation or the bootstrap, and retains the respective component only when the distribution exceeds 95 percentile. The downside of resampling is the computational burden especially when dealing with large datasets.

The number of PCs selected for the three categories of sEMG datasets by various schemes is marked in Fig. 4. As can be noticed, the criterion based on eigenvalues exceeding one failed to produce reliable results for the sEMG data related to the IMR and HC hand gestures. It is quite reasonable to retain only the PCs that could explain more than 80% of

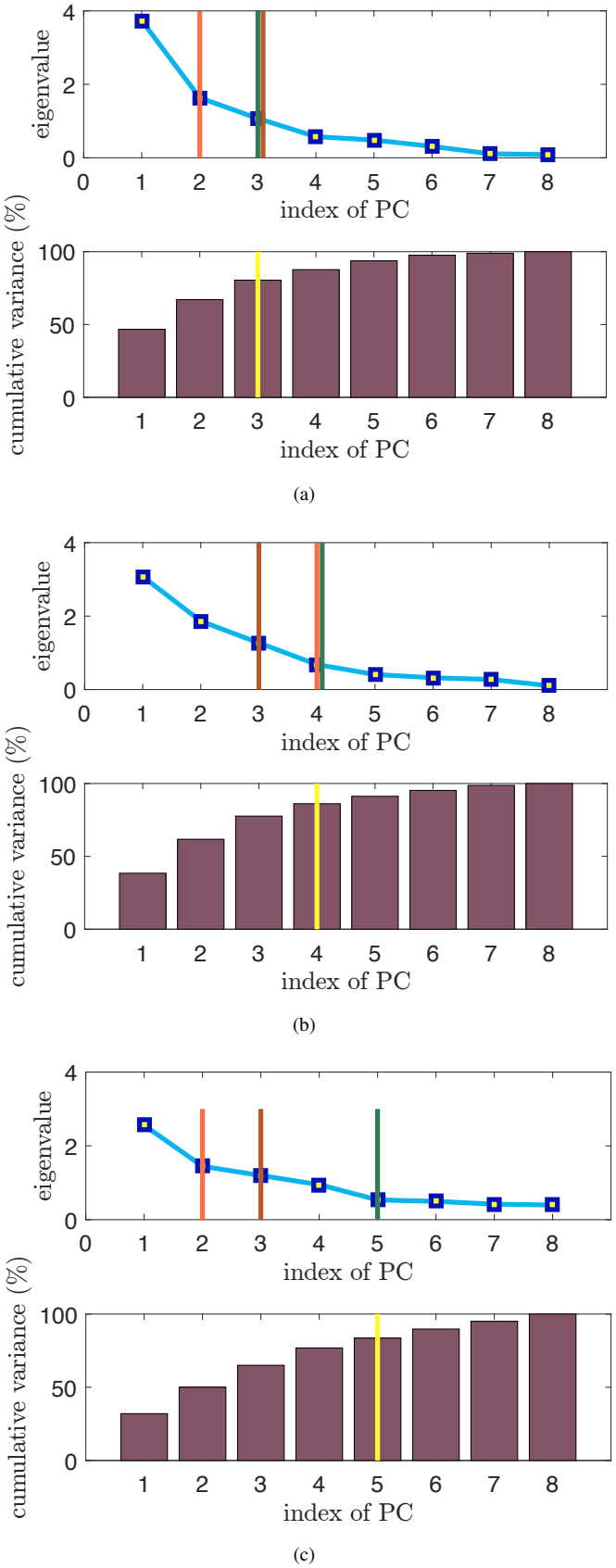

Fig. 4. Comparison of PC selection methodologies, which are based on the eigenvalues (brown marker), visual detection of the elbow (green marker), segmented-regression-based elbow estimation (orange marker), and cumulative variance explained by the PCs (yellow marker), were implemented with sEMG datasets related to three hand gesture movements: (a) middle finger, (b) IMR fingers, and (c) HC position.

TABLE I
EIGENVALUES AND EXPLAINED VARIANCES (IN %) ASSOCIATED WITH THE EIGHT PCS DERIVED FROM EACH OF THE FOLLOWING SEMG HAND GESTURE MOVEMENT DATASETS: MIDDLE FINGER, IMR FINGERS, AND HC POSITION

principal component	middle finger movement		IMR finger movement		HC position movement	
	eigenvalue	variance explained in %	eigenvalue	variance explained in %	eigenvalue	variance explained in %
PC_1	3.734	46.684	3.076	38.450	2.558	31.968
PC_2	1.633	20.414	1.863	23.287	1.447	18.089
PC_3	1.070	13.379	1.271	15.887	1.197	14.960
PC_4	0.575	7.193	0.681	8.514	0.949	11.857
PC_5	0.482	6.028	0.410	5.121	0.536	6.696
PC_6	0.310	3.879	0.321	4.009	0.497	6.215
PC_7	0.109	1.366	0.275	3.438	0.419	5.233
PC_8	0.085	1.057	0.104	1.295	0.398	4.979

the data variation to reduce the dimensionality of the sEMG data. An interesting inference from this outcome is that unlike the simple task involving the middle finger movement that requires merely three PCs, more intricate movements with IMR fingers and HC position necessitate four and five PCs, respectively. Despite being subjective, the elbow estimated by visual scrutiny supports the retention of the same number of PCs as endorsed by the principle insisting on more than $\gamma\%$ of cumulative variance explained by the reduced set of components. Since automatic detection of elbow in a scree-plot is on the rise, we intended to evaluate such a procedure, namely, *piecewise* or *segmented regression*. This algorithm traverses along the curve, and selects one bisection point at a time for fitting two line segments in the following manner: the first one is constructed such that it provides the best fit for the series of points to the left of the bisection point, while the second one takes into account the points to the right. The bisection point which minimizes the sum of errors for the two fits is construed as the elbow of the scree-plot. For the tested sEMG data falling under the hand gesture categories, i.e., the middle finger, IMR fingers, and HC position, the automatic scheme favors the choice of two, four, and two PCs, respectively, as indicated in Fig. 4.

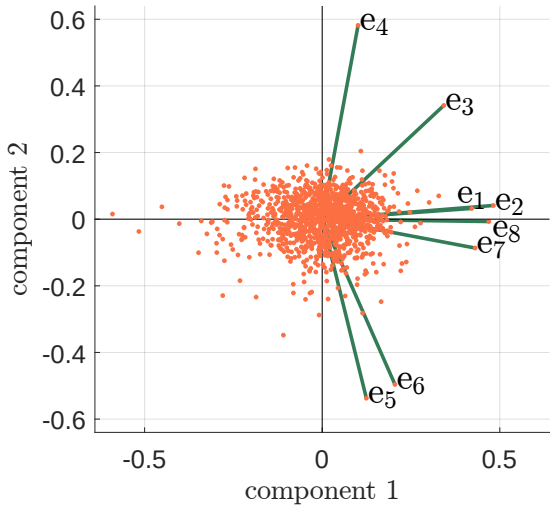

Fig. 5. Biplot of the sEMG data acquired during the middle finger movement. The horizontal and vertical axis represent the first and the second PC, respectively. The orange dots denote the scaled PC scores. The variables of the sEMG data, i.e., surface electrodes, are marked with green line segments that emanate from the origin. The plot provides information on how each variable contributes to the two PCs.

The biplot in Fig. 5 shows the first two PC scores and the loading vectors for the EMG data collected using eight electrodes, $e_1, \ldots, e_8$, during the middle finger movement. The electrodes were placed on the muscles in the following manner: e_1 ▶ *extensor digitorum* (ED); e_2, e_3 ▶ *brachioradialis* (BR); e_4 ▶ *flexor carpi radialis* (FCR); e_5, e_6, e_7 ▶ *flexor carpi ulnaris* (FCU); and e_8 ▶ *extensor carpi ulnaris* (ECU). The PC scores are scaled with respect to the maximum score value and maximum coefficient length, so that their relative locations can be determined from the plot. What one may possibly infer from the biplot is that the first loading vector places almost equal weight on the variables (electrodes) designated as e_1, e_2, e_7, and e_8, moderate weight on e_3, and less weight on the rest of the electrodes. On the contrary, the second loading vector assigns more weight on the electrodes, namely, $e_3, \ldots, e_6$, and less weight on the remaining. Based on the orientation of vectors (green line segments) that represent the variables, we speculate that the MUAPs picked up by the set of electrodes e_1, e_2, e_7, and e_8 would share some common information in the subspace spanned by PC_1 and PC_2, and the recordings by the rest of the electrodes might distinctly differ from the former ones.

IV. PCA-BASED SEMG ANALYSES

Several sEMG studies rely on the PCA to interpret muscle activation patterns and better understand the complex coordination of muscle activities in the human body. These studies have mainly focused on the following three aspects: (i) to measure redundancies, (ii) to identify patterns of coordination, and (iii) to discriminate different activities. In the subsequent section, an overview of PCA-based sEMG applications is attempted, wherein an exhaustive collection of related methods are tabulated to provide a comprehensive review on this subject.

TABLE II
MUSCLE STRENGTH AND FATIGUE ASSESSMENT

Reported study	Sensors and muscles involved	Subjects	Approaches aside from PCA & metrics used	sEMG assessment	Results/Findings	Conclusion
Staudenmann *et al*. [16]	Sensors: 63 monopolar cloth series electrodes (Kendall, Boston, USA). Muscle: *biceps brachii* (BB).	11 healthy men: age 27.3±8.3 yrs; weight 82.5±12.8 kg; and height 1.8±0.7 m.	sEMG-based force estimates using root mean square difference (RMSD)	The sEMG-based muscle activation estimates were assessed by elbow flexion forces in isometric, two-state isotonic contractions.	PCA-processed sEMG yielded more accurate estimates of muscle activation (12%–22%) than multiple bipolar sEMG using the same monopolar channels.	PCA processing of multi-channel sEMG from the BB muscle substantially improves the quality of muscle activation estimates compared to the conventional bipolar sEMG.
Rogers and MacIsaac [45]	Sensors: 8 channel Ag/AgCl electrode strip with 5 mm spacing. Muscle: BB.	9 healthy subjects	Sensitivity to variability ratio (SVR), linear PCA (LPCA), non-linear PCA (NLPCA), and end to end (ETE) projection.	Static, cyclic, and random fatiguing contractions (dynamic contractions) of the BB muscles were assessed by the SVR and PCA.	No statistical difference among ETE, PCA, and LPCA ($p > 0.99$) and all the three approaches outperformed NLPCA ($p < 0.0022$).	The performance of linear methods—ETE, PCA, and LPCA—is better than NLPCA. The proposed PCA method is very useful in identifying cyclic and dynamic muscle contractions.
Staudenmann *et al*. [53]	Sensors: active high-density sEMG grid with 13×10 electrodes (BIOSEMI, Amsterdam). Muscle: *triceps brachii* (TB).	11 healthy subjects: age 28.0±4.1 yrs; weight 67.6±9.4 kg; and height 1.8±0.1m.	RMSD	The effect of different bipolar configuration directions on the PCA and sEMG-based force estimation was studied during elbow extension.	PCA reduced the RMSD by around 40% and 12% compared to the conventional bipolar electrodes and the optimally aligned multiple bipolar electrodes, respectively.	PCA has the potential to extract relevant force-related information from a high-density sEMG grid apart from improving the quality of muscle force estimation and the accuracy of sEMG-based estimation.
Güler and Koçer [54]	Sensors: 2 sEMG bar electrodes (40 mm and 20 mm sensory bar electrode for adults and children, respectively). Muscles: *biceps* and *hypothenar group*.	59 subjects with a mean age of 28±0.5 yrs: 19 healthy, 20 myopathic, and 20 neuropathic.	Discrete Fourier transform (DFT) and fast Fourier transform (FFT).	Muscle activities of normal, myopathic, and neuropathic subjects were analyzed.	FFT coefficients from subjects with neuromuscular disorder were reduced using the PCA and classified by the support vector machine (SVM) and multilayer perceptron (MLP). The results reported 85.42% accuracy.	PCA-based approach facilitates faster diagnosis of neuromuscular disorders.
Larivière *et al*. [55]	Sensors: 12 surface electrodes (DE02, Delsys). Muscles: *lumbar* and *thoracic erector spinae*, *latissimus dorsi*, *rectus abdominis*, *external* and *internal oblique*.	33 male volunteers with 18 control subjects: age 39±3 yrs; height 1.75±0.06 m; weight 74±10 kg; and body mass index (BMI) 24.2±2.6 kg m^2. 15 patients: age 40±4 yrs; height 1.72±0.06 m; weight 69±8 kg; and BMI 23.2±2.3 kg m^2.	Reference PCA model, PCA-based distance measures, and intraclass correlation coefficients.	The sEMG waveforms of 12 trunk muscles from standardized trunk motions were studied to evaluate the reliability and sensitivity of PCA-based distance measures to the load lifted, trunk range of motion, and low back status.	PCA-based distance measures demonstrated acceptable reliability for the agonist muscles, and were sensitive to task modalities.	PCA could be a promising clinical tool to assess sEMG waveforms of trunk muscles during dynamic tasks.

TABLE III
GESTURE RECOGNITION AND PROSTHETIC APPLICATIONS

Reported study	Sensors and muscles involved	Subjects	Approaches aside from PCA & metrics used	sEMG assessment	Results/Findings	Conclusion
Xing *et al.* [24]	Sensors: 4 pairs of Ag/AgCl electrodes. Muscles: *extensor carpi radialis* (ECR), ED, *palmaris longus* (PL), and FCU.	– NA –	Wavelet packet transform (WPT), SVM, and kernel PCA (KPCA).	7 type of wrist motions: stillness, wrist extension, wrist flexion, ulna deviation, radial deviation, hand close, and hand open.	The KPCA using a Gaussian kernel outperformed the linear PCA, whereas the KPCA with a multinomial kernel failed to perform well.	The WPT and the feature dimensionality reduction by the PCA lead to an improved classification accuracy of 97%.
Li *et al.* [15]	Sensors: 6 sEMG sensors. Muscles: PL, *flexor digitorum superficialis* (FDS), *flexor digitorum profundus* (FDP), *extensor digitorum communis* (EDC), *extensor digiti minimi* (EDM), and *extensor pollicis longus* (EPL).	2 subjects	Mean absolute value (MAV), slope change, zero crossings (ZC), and SVM.	Subjects were asked to grasp 12 objects of different size and shape: apple, matchbox, 500 ml bottle, pop can, mouse, box, tea caddy, cell phone, pen, cup, spanner, and key.	PCA was applied to reduce the dimension of the human hand motion with more than 20 DoF, and the support vector regression (SVR) machine was adopted to establish the connection between sEMG signals and the low-dimensional hand postures.	PCA coupled with other techniques enables the proportional and simultaneous estimation of hand postures.
Zhang *et al.* [17]	Sensors: 4 sEMG sensors (MyoScan, Thought Technology, Canada).	– NA –	LDA, MAV, RMS, ZC, waveform length (WL), slope sign changes (SSC), power spectral density (PSD), median frequency (MF), and autoregressive coefficients (AR).	5 hand motions were assessed: hand closing, hand opening, index finger pinching, middle finger pinching, and hand relaxing.	Features were classified with an average accuracy of 99.8% by the PCA and LDA.	The classification accuracy of extracted features from sEMG signals can significantly be improved with the PCA.
Erkilinc and Sahin [56]	Sensors: 4 channel sEMG sensors (BioRadio150, Cleve Med). Muscles: ED, ECR, PL, and FCU.	3 subjects	FFT, simple PCA (sPCA), and multi-class SVM.	5 wrist movements: right, left, up, down, and relaxation.	The sEMG data preprocessed by the sPCA were classified using the multi-class SVM with 81% accuracy.	The classification performance of multiclass SVM is significantly improved due to the pre-processing carried out with the sPCA.
Matrone *et al.* [23]	Human-sized robot hand consisting of 5 underactuated anthropomorphic fingers	– NA –	Grasping trajectories	A PCA-based algorithm drove an underactuated prosthetic hand having 16 DoFs with a 2-dimensional control input to perform the 3 prehensile forms.	Design of a PCA-based control algorithm to drive an underactuated prosthetic hand with 16 DoFs and 6 degrees of moment (DoMs).	This research pursuit may open up avenues for the development of an intuitively controllable hand prosthesis.

Reported study	Sensors and muscles involved	Subjects	Approaches aside from PCA & metrics used	sEMG assessment	Results/Findings	Conclusion
Hargrove *et al*. [57]	Sensors: 10 adhesive duotrodes. Muscles: forearm of the wrist muscles, i.e., *medial, formal, dorsal*, and *lateral*.	10 healthy and 5 long traumatic transradial amputees.	AR feature set, uncorrelated LDA (ULDA) feature reduction, and LDA classifier.	11 types of gestures: wrist pronation/supination, wrist flexion/extension, hand open, key grip, chuck grip, power grip, fine pinch grip, tool grip, and a rest class.	Prior to classification, sEMG data were projected onto class-specific PCA transformation matrices for tuning, which resulted in a significant reduction of classification error ($p < 0.01$).	Pre-processing of features by the PCA significantly reduces classification errors for both intact-limbed and amputee subjects.
Kiatpanichagij and Afzulpurkar [58]	Sensors: 4 sEMG electrodes. Muscles: forearm above the *wrist flexors* and *extensors*, and on each side of the forearm.	12 normal limb subjects.	Fast correlation-based filter (FCBF), supervised discretization method coupled with PCA (sdPCA), WPT, minimal description length principle (MDLP), and artificial neural network (ANN).	6 classes of motion: hand closed, hand open, wrist flexion, wrist extension, ulnar deviation, and radial.	Pre-processed signal by the sdPCA and other features demonstrated a classification accuracy of 93.30±2.42%.	A performance enhancement is noticed owing to the application of PCA that might have circumvented the "curse of dimensionality" issue efficiently.
Matsumura *et al*. [26]	Sensors: 4 channel dry Ag/AgCl sEMG electrodes. Muscles: forearm muscles.	3 male subjects of age 21, 22, and 30 yrs.	Multi discriminant analysis (MDA), gradual PCA (gPCA), and sPCA.	7 wrist actions: relaxation, up, down, bend to right, bend to left, twist of inside, and twist of outside.	The hybrid PCA recognized the 7 wrist actions with a higher accuracy (>85%).	The PCA-based pattern recognition approach is effective in improving the gesture recognition accuracy, and it reduces the learning-time of the system.
Chu *et al*. [59]	Sensors: 4 sEMG electrodes (DE-2.1, DELSYS). Muscles: ED, ECR, PL, and FCU.	10 normal subjects: 6 males and 4 females of age 31±4.3 yrs.	WPT, local discriminant basis, and self-organizing feature map (SOFM).	9 kinds of hand motions: flexion, extension, radial flexion, ulnar flexion, pronation, and supination of the wrist; opening and grasping of the fingers; and relaxation.	The dimensionality reduction of the wavelet packet features by the PCA rendered a classification accuracy of 95% for the 9 types of motions; consequently, the virtual hand could be controlled in real time.	The improved classification accuracy, simplified classifier design, and expedited pattern recognition task are attributed to the dimensionality reduction via PCA.

Reported study	Sensors and muscles involved	Subjects	Approaches aside from PCA & metrics used	sEMG assessment	Results/Findings	Conclusion
Du *et al.* [60]	Sensors: 7 channel sEMG electrodes. Muscles: located at the right forearm, 5 cms below the elbow.	12 subjects: 9 males and 3 females with an average age of 24±3 yrs.	sEMG envelope energy, ICA, stationary wavelet transform, and neural network.	11 hand motions: flexion up, flexion down, pronation, supination, and the following extensions of fingers, i.e., index finger, thumb, index and middle fingers, thumb and little fingers, thumb and index fingers, all fingers except the thumb, and all five fingers.	The PCA led to the reduction of the neural network size by more than 70%.	The PCA remains as an effective pre-processing method for the sEMG analysis. Furthermore, it reduces the size of the neural network and increases the discrimination rate for different hand motions.
Matsumura *et al.* [61]	Sensors: 4 channel dry sEMG electrodes.	– NA –	FFT and back propagation (BP) neural network.	7 wrist actions: relaxation, up, down, bend to right, bend to left, twist of inside, and twist of outside.	The sEMG gestures, processed by the sPCA, were efficiently classified by the BP neural network.	The sPCA promotes the classification accuracy of sEMG signals acquired with 7 different wrist gestures.

TABLE IV
GAIT AND HUMAN MOVEMENT APPLICATIONS

Reported study	Sensors and muscles involved	Subjects	Approaches aside from PCA & metrics used	sEMG assessment	Results/Findings	Conclusion
Huber *et al.* [62]	Sensors: 6 bipolar Ag/AgCl sEMG electrodes (Noraxon, U.S.A.). Muscles: *rectus femoris* (RF), *vastus medialis* (VM), *vastus lateralis* (VL), *biceps femoris* (BF), and *semitendinosus* (ST).	10 healthy female volunteers (age 48±7 yrs; weight 61.1±4.9 kg; height 1.64±0.05 m) with no neurological or musculoskeletal impairments.	Time-frequency analysis and wavelets.	Both intra-subject and inter-subject variabilities of sEMG signals from the knee muscle were assessed during heel strike.	In all cases, the shapes of the first and second PCs agreed well with the predicted waveforms, and accounted for 50–60% of the overall variability, in both the inter-subject and intra-subject analyses.	The structure within a muscle activation pattern is not randomly organized. A significant fraction of the variability can be explained by a linear combination of distinct activation patterns.
Wilson *et al.* [63]	Sensors: 8 Ag/AgCl sEMG electrodes (.79 mm^2 contact area, Bortec Inc, Calgary). Muscles: VL, VM, BF, *semimembranosus*, *lateral semitendinosus* (LG), and *medial gastrocnemius* (MG).	40 individuals with mild to moderate, clinically diagnosed medial-compartment knee osteoarthritis (OA).	Pearson correlation and statistical parameters.	The association between the biomechanical as well as the neuromuscular factors of clinically diagnosed mild to moderate knee OA and the radiographic or pain severity was determined.	The first 3 PCs cumulatively represented more than 80% of the total variability in the original measure.	A combination of PCs, the knee adduction moment, and the BMI better explain the structural knee OA severity than any one of the individual factors.

Reported study	Sensors and muscles involved	Subjects	Approaches aside from PCA & metrics used	sEMG assessment	Results/Findings	Conclusion
Klarner *et al*. [64]	Sensors: 6 bipolar sEMG electrodes. Muscles: *tibialis anterior* (TA), MG, LG, *soleus* (Sol), VM, RF, VL, BF, and ST.	8 healthy subjects: 4 male and 4 female with no neurological disorders; age 22–38 yrs; height 177.63±8.72 cm; and weight 71.0±6.35 kg.	Wavelet	The extent to which the body weight support and stride frequency contribute and interact in order to produce the coordination patterns of the leg muscles was quantified.	The first PC alone accounted for 23% to 57% of the overall sEMG signal across individuals, whereas the first 5 PCs explained 56% to 81% of the total signal variance.	The sEMG coordination patterns pertaining to higher levels of body weight support and faster stride frequencies remain similar to those associated with lower levels of body weight support and slower stride frequencies.
Hubley-Kozey *et al*. [65]	Sensors: 8 channel Ag/Ag-Cl sEMG electrodes (Bortec Inc, Calgary). Muscles: 3 *quadriceps* muscles, 2 *hamstrings*, and right & left *gastrocnemii*.	78 subjects: 38 normal and 40 with OA.	Filtering	The sEMG patterns from normal and OA subjects were explored.	Pattern recognition techniques were used to investigate both amplitude and shape changes of the sEMG signals from 7 muscles crossing the knee joint of normal and OA subjects engaged in a walking task. The principal patterns for each muscle group explained more than 83% of the variance in the signals.	The principal neuro-muscular patterns of asymptomatic controls are similar to those with OA, revealing specific roles of the major muscle groups while walking. However, the mechanical environment and pain may induce subtle differences in neuromuscular responses between the two groups in a gait cycle.
Lamoth *et al*. [66]	Sensors: a pair of Ag/AgCl sEMG electrodes (Blue sensor N-00-S, Medicotest, Denmark). Muscle: *erector spinae* (ES).	19 individuals with non-specific low back pain (LBP) and 14 healthy controls.	Hilbert transform	The effect of walking velocity on the global trunk coordination and the ES activity as well as their variability were examined to understand the consequences of non-specific LBP on gait.	The global pattern of ES muscle activity deviated markedly from the normal pattern. The significant variability of the former implied a poor coordination of the ES muscle activation.	The slower walking of the LBP participants is presumably a functional adaptation to altered motor control, and may not be related to actual pain, fear of movement/re-injury or level of disability.
Krishnamoorthy *et al*. [67]	Sensors: disposable self-adhesive electrodes (3 M). Muscles: TA, *gastrocnemius lateralis* (GL), *gastrocnemius medialis* (GM), Sol, VL, VM, RF, BF, ST, *rectus abdominis* (RA), and ES.	8 healthy subjects: 4 male and 4 female without neurological/motor disorder; age 29±4.5 yrs; weight 60.63±7.2 kg; and height 1.68±0.1 m.	Uncontrolled manifold (UCM) and multiple regression.	PCA was used along with the UCM to identify 11 postural muscle synergies during various postural tasks at different speeds.	Each of the 3 identified PCs represented a "muscular" pattern, i.e., levels of simultaneous activation of all the 11 muscles.	The center of pressure shifts are controlled by a small set of central variables, while each of the variables induces changes in the activity of a subgroup of postural muscles.

TABLE V
PCA FOR FACIAL sEMG APPLICATIONS

Reported study	Sensors and muscles involved	Subjects	Approaches aside from PCA & metrics used	sEMG assessment	Results/Findings	Conclusion
Jerritta *et al*. [68]	Sensors: facial electromyography (fEMG) electrodes. Muscle: *zygomaticus major* (ZM).	Healthy volunteers: 8 male and 7 female with ages ranging from 18 to 25 yrs.	K-nearest neighbors algorithm, mean and SD of the raw signal, mean absolute value of first and second differences of the signal, skewness, and kurtosis.	6 emotional states—*happy, sad, fear, surprise, neutral, and disgust*—were recognized using the fEMG signals.	The PCA-based feature vector reduction was found to improve the emotion recognition rate.	The features pre-processed by the PCA enhance the classification accuracy.
Andrade *et al*. [69]	Sensors: 2 pairs of Ag/AgCl electrodes. Muscles: left & right *temporalis and frontalis*.	11 subjects: 10 healthy and 1 suffering from muscular dystrophy.	Finite state machine (FSM), MAV, and autocorrelation.	7 commands—*single click, up, down, left, right, rotate, and on standby*—used for the control of the cursor on a computer screen were recognized with fEMG signals.	PCA was applied to the data acquired from all the subjects, and the 2 most relevant PCs were selected based on the data variability explained by each of them.	An fEMG-based human computer interface is introduced for the mouse cursor control with the aid of PCA and FSM, wherein the role of PCA is to enable the visualization of differences among subjects.
Zhou *et al*. [18]	Sensors: 5 duotrode bipolar Ag/AgCl electrodes. Muscles: *levator anguli oris, zygomaticus, platysma, depressor anguli oris*, and anterior belly of *digastric*.	6 subjects	Mel-frequency cepstral coefficient (MFCC), time domain features, and Gaussian mixture model.	10 phonemes, starting from 0 to 9, were classified.	The data reduced by the PCA were classified via a hidden Markov model (HMM), which resulted in an average word classification accuracy of 98.53% over 6 subjects.	Pre-processing of the myoelectric signals using a class-specific PCA has been shown to improve the ability of an HMM classifier that recognizes phonemes by an average of 4%.
Jia *et al*. [70]	Sensors: 3 sEMG electrodes. Muscles: ZM and anterior belly of *digastric*.	1 subject	Wavelet transform, AR model, cepstral coefficients, and BP-ANN.	6 Chinese vowels, namely, /a/, /o/, /e/, /i/, /u/, and /ű/, were studied.	For the 6 Chinese vowels, the PCA-processed BP networks produced an average classification rate of 77.3%, while the vowels, /ű/ and /i/, were classified with an accuracy of more than 90%.	An efficient classifier is propounded by combining two BP network classifiers, which is supplied with the reduced feature set by the PCA. The feature reduction contributes to the improvement in the classification rate of BP-ANN.

V. Conclusions and Perspectives

The purpose of this article is to provide an overview of the literature reported on the PCA application to process the sEMG signals acquired from various muscles, especially those located in the face as well as the upper and lower limbs. In this context, the PCA has been employed as an unsupervised feature extraction scheme that reduces the dimensionality of the sEMG data to befit various myoelectric applications. Furthermore, we recounted several applications of PCA involving myoelectric signals. The main objective here is to review noteworthy references in this domain, and to offer pointers to the literature on this research trend.

Recapitulated below are the rationale behind the strong preference of PCA algorithm with relevance to the sEMG data preprocessing. In principle, the PCA identifies a common temporal pattern across large datasets of sEMG signals, and defines a low-dimensional space on which the original signals could be represented as vectors and classified [18]. In this vein, the PCA could be adopted to process the sEMG activity of individual muscles recorded during several variants of one motor action (or even different motor behaviors), and to characterize the temporal patterns of activity associated with different components of the motor action. Recollect from Section II-C that the PCs explaining a significant proportion of the data variation could be ascribed to the control signal outputs of spinal pattern generators [46]; whereas, the rest of the PCs presumably account for the system-related random noise [41]. Moreover, the PCA-based sEMG data decomposition facilitates to unravel the inherent coordinative structures in the correlated patterns of variation among joints or body segments [47], [48]. These structures corresponding to walking and gait could render valuable information on the body control mechanism, and help correlate walking patterns with injuries [48]. Another potential application of the PCA is concerned with the analysis of patterns of sEMG activity recorded via multi-electrode systems from many muscles throughout the body during one or more motor actions. In this case, the role of PCA is to identify spatial temporal neuromuscular synergies underlying the motor behavior [67].

To summarize, the PCA applications to sEMG data outlined here highlight the efficacy of this method in capturing features from sEMG signals that can provide insight not only on the activation state of motoneurons, but also on the nature of the premotor control signals, which would open new avenues for clinical, neurophysiological, and rehabilitation studies.

References

[1] W. F. Brown, *The Physiological and Technical Basis of Electromyography*. Butterworth-Heinemann, 2013.

[2] L. D. Weiss, J. M. Weiss, and J. K. Silver, *Easy EMG: A Guide to Performing Nerve Conduction Studies and Electromyography*. Elsevier Health Sciences, 2015.

[3] R. H. Chowdhury, M. B. Reaz, M. A. B. M. Ali, A. A. Bakar, K. Chellappan, and T. G. Chang, "Surface electromyography signal processing and classification techniques," *Sensors*, vol. 13, no. 9, pp. 12 431–12 466, 2013.

[4] E. Criswell, *Cram's Introduction to Surface Electromyography*. Jones & Bartlett Publishers, 2010.

[5] D. Farina, R. Merletti, and R. M. Enoka, "The extraction of neural strategies from the surface EMG," *Journal of Applied Physiology*, vol. 96, no. 4, pp. 1486–1495, 2004.

[6] T. Moritani, D. Stegeman, and R. Merletti, "Basic physiology and biophysics of EMG signal generation," *Electromyography Physiology Engineering and Noninvasive Applications*, pp. 1–20, 2004.

[7] F. Láhoda, A. Ross, and W. Issel, *EMG Primer: A Guide to Practical Electromyography and Electroneurography*. Springer Science & Business Media, 2012.

[8] R. M. Howard, R. Conway, and A. J. Harrison, "An exploration of eliminating cross-talk in surface electromyography using independent component analysis," in *Proceedings of 26th Irish Signals and Systems Conference*. IEEE, 2015, pp. 1–6.

[9] V. S. Selvanayagam, S. Riek, and T. J. Carroll, "A systematic method to quantify the presence of cross-talk in stimulus-evoked EMG responses: implications for TMS studies," *Journal of Applied Physiology*, vol. 112, no. 2, pp. 259–265, 2012.

[10] C. Bakker, A. van Kuijk, A. Geurts, D. Stegeman, and J. Pasman, "Can forearm muscle activity be selectively recorded using conventional surface EMG-electrodes in transcranial magnetic stimulation? A feasibility study," *Journal of Electromyography and Kinesiology*, vol. 24, no. 3, pp. 325–331, 2014.

[11] M. Yung and R. Wells, "Changes in muscle geometry during forearm pronation and supination and their relationships to EMG cross-correlation measures," *Journal of Electromyography and Kinesiology*, vol. 23, no. 3, pp. 664–672, 2013.

[12] M. B. Jensen, J. A. B. Manresa, K. S. Frahm, and O. K. Andersen, "Analysis of muscle fiber conduction velocity enables reliable detection of surface EMG crosstalk during detection of nociceptive withdrawal reflexes," *BMC Neuroscience*, vol. 14, no. 1, p. 39, 2013.

[13] C. J. De Luca, M. Kuznetsov, L. D. Gilmore, and S. H. Roy, "Inter-electrode spacing of surface EMG sensors: Reduction of crosstalk contamination during voluntary contractions," *Journal of Biomechanics*, vol. 45, no. 3, pp. 555–561, 2012.

[14] L. Wang, A. Lu, S. Zhang, W. Niu, F. Zheng, and M. Gong, "Fatigue-related electromyographic coherence and phase synchronization analysis between antagonistic elbow muscles," *Experimental Brain Research*, vol. 233, no. 3, pp. 971–982, 2015.

[15] S. Li, X. Chen, X. Sheng, and X. Zhu, "Preliminary study on proportional and simultaneous estimation of hand posture using surface EMG based on synergy concept," in *Proceedings of 35th Annual International Conference of the IEEE Engineering in Medicine and Biology Society*. IEEE, 2013, pp. 6199–6202.

[16] D. Staudenmann, D. F. Stegeman, and J. H. van Dieën, "Redundancy or heterogeneity in the electric activity of the biceps brachii muscle? Added value of PCA-processed multi-channel EMG muscle activation estimates in a parallel-fibered muscle," *Journal of Electromyography and Kinesiology*, vol. 23, no. 4, pp. 892–898, 2013.

[17] D. Zhang, A. Xiong, X. Zhao, and J. Han, "PCA and LDA for EMG-based control of bionic mechanical hand," in *Proceedings of International Conference on Information and Automation*. IEEE, 2012, pp. 960–965.

[18] Q. Zhou, N. Jiang, K. Englehart, and B. Hudgins, "Improved phoneme-based myoelectric speech recognition," *IEEE Trans. Biomed. Eng.*, vol. 56, no. 8, pp. 2016–2023, 2009.

[19] K.-L. Du and M. Swamy, "Principal component analysis," in *Neural Networks and Statistical Learning*. Springer, 2014, pp. 355–405.

[20] V. C. Klema and A. J. Laub, "The singular value decomposition: Its computation and some applications," *IEEE Trans. Autom. Control*, vol. 25, no. 2, pp. 164–176, 1980.

[21] A. Hyvärinen, J. Karhunen, and E. Oja, *Independent Component Analysis*. John Wiley & Sons, 2004, vol. 46.

[22] D. D. Lee and H. S. Seung, "Algorithms for non-negative matrix factorization," in *Advances in neural information processing systems*, 2001, pp. 556–562.

[23] G. C. Matrone, C. Cipriani, E. L. Secco, G. Magenes, and M. C. Carrozza, "Principal components analysis based control of a multi-dof underactuated prosthetic hand," *Journal of Neuroengineering and Rehabilitation*, vol. 7, no. 1, p. 1, 2010.

[24] K. Xing, P. Yang, J. Huang, Y. Wang, and Q. Zhu, "A real-time EMG pattern recognition method for virtual myoelectric hand control," *Neurocomputing*, vol. 136, pp. 345–355, 2014.

[25] A. Daffertshofer, C. J. C. Lamoth, O. G. Meijer, and P. J. Beek, "PCA in studying coordination and variability: A tutorial," *Clinical Biomechanics*, vol. 19, no. 4, pp. 415–428, 2004.

[26] Y. Matsumura, M. Fukumi, and Y. Mitsukura, "Hybrid EMG recognition system by MDA and PCA," in *Proceedings of International Joint Conference on Neural Networks*. IEEE, 2006, pp. 5294–5300.

[27] M. J. Zwarts and D. F. Stegeman, "Multichannel surface EMG: Basic aspects and clinical utility," *Muscle & Nerve*, vol. 28, no. 1, pp. 1–17, 2003.

[28] D. F. Stegeman, J. H. Blok, H. J. Hermens, and K. Roeleveld, "Surface EMG models: Properties and applications," *Journal of Electromyography and Kinesiology*, vol. 10, no. 5, pp. 313–326, 2000.

[29] K. T. Patton, *Anatomy and Physiology*. Elsevier Health Sciences, 2015.

[30] A. Holobar, D. Farina, and D. Zazula, "Surface EMG decomposition," *Surface Electromyography: Physiology, Engineering, and Applications*, pp. 180–209, 2016.

[31] R. Merletti and P. A. Parker, *Electromyography: Physiology, Engineering, and Non-invasive Applications*. John Wiley & Sons, 2004, vol. 11.

[32] L. Mesin, R. Merletti, and A. Rainoldi, "Surface EMG: The issue of electrode location," *Journal of Electromyography and Kinesiology*, vol. 19, no. 5, pp. 719–726, 2009.

[33] C. J. De Luca, S.-S. Chang, S. H. Roy, J. C. Kline, and S. H. Nawab, "Decomposition of surface EMG signals from cyclic dynamic contractions," *Journal of Neurophysiology*, vol. 113, no. 6, pp. 1941–1951, 2015.

[34] M. Rojas-Martínez, M. A. Mañanas, J. F. Alonso, and R. Merletti, "Identification of isometric contractions based on high density EMG maps," *Journal of Electromyography and Kinesiology*, vol. 23, no. 1, pp. 33–42, 2013.

[35] D. Farina, C. Cescon, and R. Merletti, "Influence of anatomical, physical, and detection-system parameters on surface EMG," *Biological Cybernetics*, vol. 86, no. 6, pp. 445–456, 2002.

[36] T. W. Beck, M. S. Stock, and J. M. Defreitas, "Shifts in EMG spectral power during fatiguing dynamic contractions," *Muscle & Nerve*, vol. 50, no. 1, pp. 95–102, 2014.

[37] C. J. De Luca, L. D. Gilmore, M. Kuznetsov, and S. H. Roy, "Filtering the surface EMG signal: Movement artifact and baseline noise contamination," *Journal of Biomechanics*, vol. 43, no. 8, pp. 1573–1579, 2010.

[38] D. A. Gabriel, A. Christie, J. G. Inglis, and G. Kamen, "Experimental and modelling investigation of surface EMG spike analysis," *Medical Engineering & Physics*, vol. 33, no. 4, pp. 427–437, 2011.

[39] D. Farina and R. M. Enoka, "Surface EMG decomposition requires an appropriate validation," *Journal of Neurophysiology*, vol. 105, no. 2, pp. 981–982, 2011.

[40] M. M. M. S. Hussain and M. Mamun, "Effectiveness of the wavelet transform on the surface EMG to understand the muscle fatigue during walk," *Measurement Science Review*, vol. 12, no. 1, pp. 28–33, 2012.

[41] K. J. Deluzio, U. P. Wyss, B. Zee, P. A. Costigan, and C. Serbie, "Principal component models of knee kinematics and kinetics: Normal vs. pathological gait patterns," *Human Movement Science*, vol. 16, no. 2, pp. 201–217, 1997.

[42] U. Dillmann, C. Holzhoffer, Y. Johann, S. Bechtel, S. Gräber, C. Massing, J. Spiegel, S. Behnke, J. Bürmann, and A. K. Louis, "Principal component analysis of gait in Parkinson's disease: relevance of gait velocity," *Gait & Posture*, vol. 39, no. 3, pp. 882–887, 2014.

[43] I. Jolliffe, *Principal Component Analysis*. Wiley Online Library, 2002.

[44] H. Abdi and L. J. Williams, "Principal component analysis," *Wiley Interdisciplinary Reviews: Computational Statistics*, vol. 2, no. 4, pp. 433–459, 2010.

[45] D. R. Rogers and D. T. MacIsaac, "EMG-based muscle fatigue assessment during dynamic contractions using principal component analysis," *Journal of Electromyography and Kinesiology*, vol. 21, no. 5, pp. 811–818, 2011.

[46] Y. P. Ivanenko, R. Grasso, M. Zago, M. Molinari, G. Scivoletto, V. Castellano, V. Macellari, and F. Lacquaniti, "Temporal components of the motor patterns expressed by the human spinal cord reflect foot kinematics," *Journal of Neurophysiology*, vol. 90, no. 5, pp. 3555–3565, 2003.

[47] G. Bosco, "Principal component analysis of electromyographic signals: An overview," *Open Rehabilitation Journal*, vol. 3, pp. 127–31, 2010.

[48] X. Wang, N. O'Dwyer, and M. Halaki, "A review on the coordinative structure of human walking and the application of principal component analysis," *Neural Regeneration Research*, vol. 8, no. 7, p. 662, 2013.

[49] R. N. Khushaba, S. Kodagoda, D. Liu, and G. Dissanayake, "Muscle computer interfaces for driver distraction reduction," *Computer Methods and Programs in Biomedicine*, vol. 110, no. 2, pp. 137–149, 2013.

[50] H. F. Kaiser, "A note on Guttman's lower bound for the number of common factors," *British Journal of Statistical Psychology*, vol. 14, no. 1, pp. 1–2, 1961.

[51] A. J. O'Toole, K. A. Deffenbacher, D. Valentin, and H. Abdi, "Low-dimensional representation of faces in higher dimensions of the face space," *Journal of Optical Soceity of America A*, vol. 10, no. 3, pp. 405–411, 1993.

[52] M. Zhu and A. Ghodsi, "Automatic dimensionality selection from the scree plot via the use of profile likelihood," *Computational Statistics & Data Analysis*, vol. 51, no. 2, pp. 918–930, 2006.

[53] D. Staudenmann, I. Kingma, A. Daffertshofer, D. F. Stegeman, and J. H. Van Dieën, "Improving EMG-based muscle force estimation by using a high-density EMG grid and principal component analysis," *IEEE Trans. Biomed. Eng.*, vol. 53, no. 4, pp. 712–719, 2006.

[54] N. F. Güler and S. Koçer, "Classification of EMG signals using PCA and FFT," *Journal of Medical Systems*, vol. 29, no. 3, pp. 241–250, 2005.

[55] C. Larivière, D. Gagnon, and P. Loisel, "An application of pattern recognition for the comparison of trunk muscles EMG waveforms between subjects with and without chronic low back pain during flexion–extension and lateral bending tasks," *Journal of Electromyography and Kinesiology*, vol. 10, no. 4, pp. 261–273, 2000.

[56] M. S. Erkilinc and F. Sahin, "Camera control with EMG signals using principal component analysis and support vector machines," in *Proceedings of IEEE International Systems Conference*. IEEE, 2011, pp. 417–421.

[57] L. J. Hargrove, G. Li, K. B. Englehart, and B. S. Hudgins, "Principal components analysis preprocessing for improved classification accuracies in pattern-recognition-based myoelectric control," *IEEE Trans. Biomed. Eng.*, vol. 56, no. 5, pp. 1407–1414, 2009.

[58] K. Kiatpanichagij and N. Afzulpurkar, "Use of supervised discretization with PCA in wavelet packet transformation-based surface electromyogram classification," *Biomedical Signal Processing and Control*, vol. 4, no. 2, pp. 127–138, 2009.

[59] J.-U. Chu, I. Moon, and M.-S. Mun, "A real-time EMG pattern recognition system based on linear-nonlinear feature projection for a multifunction myoelectric hand," *IEEE Trans. Biomed. Eng.*, vol. 53, no. 11, pp. 2232–2239, 2006.

[60] Y. C. Du, W. C. Hu, and L. Y. Shyu, "The effect of data reduction by independent component analysis and principal component analysis in hand motion identification," in *Proceedings of 26th Annual International Conference of the IEEE Engineering in Medicine and Biology Society*, vol. 1. IEEE, 2004, pp. 84–86.

[61] Y. Matsumura, Y. Mitsukura, M. Fukumi, N. Akamatsu, Y. Yamamoto, and K. Nakaura, "Recognition of EMG signal patterns by neural networks," in *Proceedings of 9th International Conference on Neural Information Processing*, vol. 2. IEEE, 2002, pp. 750–754.

[62] C. Huber, P. Federolf, C. Nüesch, P. C. Cattin, N. F. Friederich, and V. von Tscharner, "Heel-strike in walking: Assessment of potential sources of intra-and inter-subject variability in the activation patterns of muscles stabilizing the knee joint," *Journal of Biomechanics*, vol. 46, no. 7, pp. 1262–1268, 2013.

[63] J. L. A. Wilson, K. J. Deluzio, M. J. Dunbar, G. E. Caldwell, and C. L. Hubley-Kozey, "The association between knee joint biomechanics and neuromuscular control and moderate knee osteoarthritis radiographic and pain severity," *Osteoarthritis and Cartilage*, vol. 19, no. 2, pp. 186–193, 2011.

[64] T. Klarner, H. K. Chan, J. M. Wakeling, and T. Lam, "Patterns of muscle coordination vary with stride frequency during weight assisted treadmill walking," *Gait & Posture*, vol. 31, no. 3, pp. 360–365, 2010.

[65] C. L. Hubley-Kozey, K. J. Deluzio, S. C. Landry, J. S. McNutt, and W. D. Stanish, "Neuromuscular alterations during walking in persons with moderate knee osteoarthritis," *Journal of Electromyography and Kinesiology*, vol. 16, no. 4, pp. 365–378, 2006.

[66] C. J. C. Lamoth, O. G. Meijer, A. Daffertshofer, P. I. J. M. Wuisman, and P. J. Beek, "Effects of chronic low back pain on trunk coordination and back muscle activity during walking: Changes in motor control," *European Spine Journal*, vol. 15, no. 1, pp. 23–40, 2006.

[67] V. Krishnamoorthy, M. L. Latash, J. P. Scholz, and V. M. Zatsiorsky, "Muscle synergies during shifts of the center of pressure by standing persons," *Experimental Brain Research*, vol. 152, no. 3, pp. 281–292, 2003.

[68] S. Jerritta, M. Murugappan, K. Wan, and S. Yaacob, "Emotion recognition from facial EMG signals using higher order statistics and principal component analysis," *Journal of the Chinese Institute of Engineers*, vol. 37, no. 3, pp. 385–394, 2014.

[69] A. O. Andrade, A. A. Pereira, C. G. Pinheiro Jr., and P. J. Kyberd, "Mouse emulation based on facial electromyogram," *Biomedical Signal Processing and Control*, vol. 8, no. 2, pp. 142–152, 2013.

[70] X. Jia, X. Wang, J. Li, and Y. Du, "Unvoiced speech recognition based on one-channel facial myoelectric signal," in *Proceedings of 6th World Congress on Intelligent Control and Automation*, vol. 2. IEEE, 2006, pp. 9362–9366.